Volume 10 | Number 18 | 21 September 2023

10 YEARS ANNIVERSARY

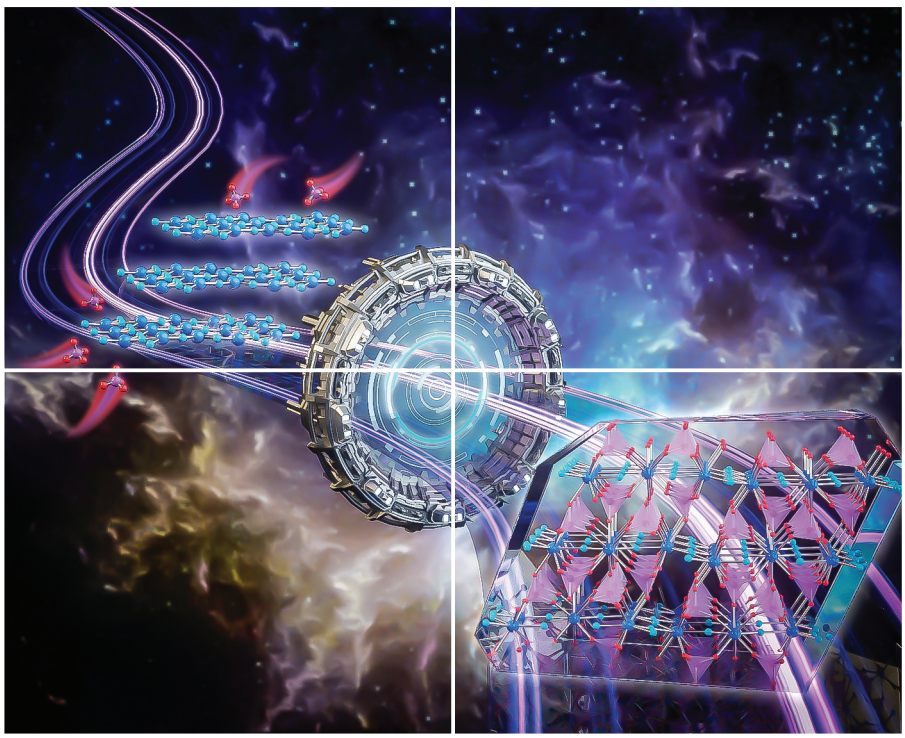

INORGANIC CHEMISTRY

FRONTIERS

CCS 中国化学会 CHINESE CHEMICAL SOCIETY
PEKING UNIVERSITY 1898
ROYAL SOCIETY OF CHEMISTRY
rsc.li/frontiers-inorganic

INORGANIC CHEMISTRY FRONTIERS

RESEARCH ARTICLE

View Article Online
View Journal | View Issue

Cite this: *Inorg. Chem. Front.*, 2023, **10**, 5270

$Ce_3F_4(SO_4)_4$: cationic framework assembly for designing polar nonlinear optical material through fluorination degree modulation†

Tianhui Wu,‡[a] Xingxing Jiang, ‡[b] Chao Wu, *‡[a] Zheshuai Lin, [b] Zhipeng Huang, [a] Mark G. Humphrey [c] and Chi Zhang *[a]

Noncentrosymmetric (NCS) structure is the paramount precondition for producing second-harmonic generation (SHG) of crystalline materials. Herein, a fluorine-enriched-induced centrosymmetric-to-non-centrosymmetric transformation strategy was employed in CS $Ce_2F_2(SO_4)_3{\cdot}2H_2O$, leading to the discovery of new NCS cerium fluoride sulfate, $Ce_3F_4(SO_4)_4$. $Ce_3F_4(SO_4)_4$ crystallizes in polar space group *C*2, and features a 2D-layered framework constructed from $[CeO_5F_3]$ and $[CeO_6F_2]$ polyhedra, extending to a final 3D framework linked *via* two crystallographically independent $[SO_4]$ units. $Ce_3F_4(SO_4)_4$ displays a phase-matchable SHG effect of about 1.0 times that of KDP and sufficient experimental birefringence (0.141@546 nm) in fluorine-containing sulfate-based NLO materials. Structural analysis and first-principle calculations suggest that the ordered arrangement of fluorinated cerium-centered polyhedra ($[CeO_5F_3]$ and $[CeO_6F_2]$) as well as $[SO_4]$ tetrahedra play a significant role in SHG activity and birefringence. Our study illustrates that the introduction of metal-centered polyhedra with a high degree of fluorination is conducive to the formation of NCS structure and is a valuable method for designing novel nonlinear optical materials.

Received 18th March 2023,
Accepted 1st May 2023

DOI: 10.1039/d3qi00513e

rsc.li/frontiers-inorganic

Introduction

Nonlinear optical (NLO) materials with second-harmonic generation (SHG) properties have important applications in advanced laser technology owing to their frequency conversion abilities.[1–8] A series of state-of-the-art NLO crystals has been used practically from the ultraviolet (UV) region to the infrared (IR) region, as exemplified by $KBe_2B_2O_6F_2$ (KBBF),[9] LiB_3O_5 (LBO),[10] $LiNbO_3$,[11] $KTiOPO_4$ (KTP),[12] and $AgGaQ_2$ (Q = S, Se).[13] The paramount precondition for producing a SHG response is the crystallographic noncentrosymmetric (NCS) structure of crystalline materials.[14–17] Unfortunately, inorganic crystals are inclined to form centrosymmetric (CS) structures in ICSD, and NCS materials make up only one-fifth of the total. Thus, applicable strategies to increase the incidence of NCS structures for designing new NLO crystals are consequently a hot research topic and of commercial interest.

To date, fluoride modulation has been reported as an applicable route for designing NLO crystals, which has been adopted to enhance additive polarization of acentric units.[18–25] Generally, fluoride modulation is grouped into two categories based on different replacement modes: (1) fluorinated metal-centered polyhedra with M–F bonds, such as $BiFSeO_3$,[26] $BiF_2(IO_3)$,[27] $CsSbF_2SO_4$,[28] and $K_5(W_3O_9F_4)(IO_3)$;[29] and (2) fluorinated anionic groups, such as fluorooxoborates consisting of B–F bonds, fluoroiodates consisting of I–F bonds, and fluorophosphates consisting of P–F bonds, as exemplified by $PbB_5O_7F_3$,[30] BiB_2O_4F,[31] $CsIO_2F_2$,[32] and $(NH_4)_2PO_3F$.[33] Although the introduction of fluoride has been widely used for developing NLO materials, many CS structures are still produced; relevant examples include $LiGaF_2(IO_3)_2$,[34] $Ba(IO_2F_2)_2$,[35] $K_4(PO_2F_2)_2(S_2O_7)$,[36] and $Cs_6Sb_4F_{12}(SO_4)_3$.[37] To our best knowledge, previous fluoride modulation studies have mainly focused on constructing a highly asymmetric group for enhancing microscopic polarizability. There is still a great lack of studies for rational understanding of the fluoride modulation process, which is considerably significant and extremely urgent.

In this study, we have focused on tetravalent rare-earth cerium fluoride sulfates due to a unique coordination environ-

[a]*China-Australia Joint Research Center for Functional Molecular Materials, School of Chemical Science and Engineering, Tongji University, Shanghai 200092, China. E-mail: chizhang@tongji.edu.cn, wuc@tongji.edu.cn*
[b]*Key Laboratory of Functional Crystals and Laser Technology, Technical Institute of Physics and Chemistry, Chinese Academy of Sciences, Beijing 100190, China*
[c]*Research School of Chemistry, Australian National University, Canberra, Australian Capital Territory 2601, Australia*

†Electronic supplementary information (ESI) available: Details of crystallographic data, measurements of physical properties, and theoretical calculations. CCDC 2179763 and 2179764. For ESI and crystallographic data in CIF or other electronic format see DOI: https://doi.org/10.1039/d3qi00513e

‡These authors contributed equally to this work.

ment and localized 4f electrons of the Ce^{4+} cation,[38–40] and a new compound, $Ce_2F_2(SO_4)_3{\cdot}2H_2O$, with a 1D $[CeF]_\infty$ chain-like framework, was obtained first while it unexpectedly crystallized in CS nonpolar space group *Pbcn* because of counteraction of microscopic polarizations. Based on the fluorination degree modulation method, a cationic framework assembly strategy was thus first achieved by using F^- anions as "tailors" to sew the 1D $[CeF]_\infty$ linear chains in $Ce_2F_2(SO_4)_3{\cdot}2H_2O$ for the creation of a 2D $[Ce_3F_4]_\infty$ layer in $Ce_3F_4(SO_4)_4$, eventually leading to the construction of a new NCS polar cerium fluoride sulfate, $Ce_3F_4(SO_4)_4$, based on the CS nonpolar parent compound $Ce_2F_2(SO_4)_3{\cdot}2H_2O$. Accordingly, 1D $[CeF]_\infty$ linear chains induce the polarization of Ce-centered polyhedra and $[SO_4]$ units in $Ce_2F_2(SO_4)_3{\cdot}2H_2O$ to be cancelled out completely by each other, while a 2D $[Ce_3F_4]_\infty$ layer not only makes Ce-centered polyhedra have a highly distorted coordination environment but also further assembles $[SO_4]$ groups in the ordered arrangement, eventually resulting in the construction of NCS rare-earth metal cerium fluoride sulfate $Ce_3F_4(SO_4)_4$. Notably, $Ce_3F_4(SO_4)_4$ exhibits a large SHG effect of about 1.0 × KDP and sufficient birefringence (0.096@1064 nm) in fluorine-containing sulfate-based NLO materials. This work proves that structural regulation realized *via* fluorination degree modulation can serve as a guide in designing new structure-driven NLO materials.

Experimental section

Reagents

CeO_2 (99.99%, Xiya Reagent), SrF_2 (99.5%, Adamas Reagent), H_2SO_4 (98 wt%, Sinopharm Chemical Reagent), and HF (40 wt%, Tansoole Chemical Reagent) were commercially available and were used directly.

Synthesis of $Ce_2F_2(SO_4)_3{\cdot}2H_2O$ and $Ce_3F_4(SO_4)_4$

Polycrystalline samples of $Ce_2F_2(SO_4)_3{\cdot}2H_2O$ were obtained *via* a conventional hydrothermal reaction with the following reaction process: $2CeO_2 + 3H_2SO_4 + 2HF \rightarrow Ce_2F_2(SO_4)_3{\cdot}2H_2O + 2H_2O$. The constituent components are shown below: CeO_2 (0.241 g, 1.4 mmol), H_2SO_4 (0.5 mL), HF (80 μL), and deionized water (1.0 mL). The polycrystalline samples of $Ce_3F_4(SO_4)_4$ can also be successfully synthesized by a mild hydrothermal reaction: $3CeO_2 + 4H_2SO_4 + 2SrF_2 \rightarrow Ce_3F_4(SO_4)_4 + 4H_2O + 2SrO$. The constituent components are shown below: CeO_2 (0.138 g, 0.8 mmol), H_2SO_4 (0.4 mL), SrF_2 (0.126 g, 1.0 mmol), and deionized water (1.0 mL). The mixed solutions were separately sealed in a 23 mL autoclave with a Teflon liner at 230 °C for 4 days, and then slowly cooled to 30 °C at a rate of 4 °C h^{-1}. After washing and drying in air, two kinds of yellow block-like crystals were obtained with yields of 55% and 65% of $Ce_2F_2(SO_4)_3{\cdot}2H_2O$ and $Ce_3F_4(SO_4)_4$, respectively (based on Ce). It is noteworthy that different fluoride sources (such as HF and some divalent metal fluorides) applied as the starting materials in the syntheses may lead to various cerium sulfate fluorides with different components.[39] The result indicates that the starting material SrF_2 used in the study not only acts as a fluoride source but also serves as the structure directing agent in the synthesis of $Ce_3F_4(SO_4)_4$.

Structural determination

A Bruker D8 VENTURE CMOS X-ray diffractometer with Mo-Kα radiation (λ = 0.71073 Å) was used for collecting and reducing the single-crystal XRD data of $Ce_2F_2(SO_4)_3{\cdot}2H_2O$ and $Ce_3F_4(SO_4)_4$ through employing APEX II software. The absorption corrections were further acquired with the multiscan-type model. The structures of $Ce_2F_2(SO_4)_3{\cdot}2H_2O$ and $Ce_3F_4(SO_4)_4$ were determined through direct methods and refined on F^2 by full-matrix least-squares methods utilizing SHELXTL-97.[41] All atoms were refined anisotropically and the PLATON[42] was applied to check for missing symmetry elements; none was found. Key crystallographic information for $Ce_2F_2(SO_4)_3{\cdot}2H_2O$ and $Ce_3F_4(SO_4)_4$ are summarized in Table 1 and detailed crystallographic data are listed in Tables S1–S5.†

Powder X-ray diffraction

The PXRD patterns of two title compounds were recorded in the Bruker D8 X-ray diffractometer with Cu-Kα radiation (λ = 1.5418 Å) in a 2θ range of 5–70° (step size: 0.02°).

Energy-dispersive X-ray spectroscopy (EDS)

Elemental analyses were carried out on a scanning electron microscope with EDS (Hitachi S-4800, Japan), which demon-

Table 1 Crystallographic data and refinement parameters for $Ce_2F_2(SO_4)_3{\cdot}2H_2O$ and $Ce_3F_4(SO_4)_4$

Formula	$Ce_2F_2(SO_4)_3{\cdot}2H_2O$	$Ce_3F_4(SO_4)_4$
Formula weight	642.48	880.60
Temperature (K)	293(2) K	293(2) K
Crystal system	Orthorhombic	Monoclinic
Space group	*Pbcn*	*C*2
a (Å)	21.8658(8)	12.0820(11)
b (Å)	6.5623(2)	5.5974(5)
c (Å)	8.2248(3)	10.7886(9)
α (°)	90	90
β (°)	90	96.773
γ (°)	90	90
V (Å^3)	1180.18(7)	724.52(11)
Z	4	2
ρ_{calc} (g cm^{-3})	3.616	4.037
μ (mm^{-1})	8.255	9.980
F (000)	1192	804
θ (°)	4.08–27.11	3.40–27.11
limiting indices	$-28 \le h \le 28$, $-8 \le k \le 8$, $-10 \le l \le 9$	$-15 \le h \le 15$, $-7 \le k \le 6$, $-13 \le l \le 13$
R_{int}	0.0267	0.0241
Reflections collected/unique	6596/1301	6641/1569
goodness of fit on F^2	1.259	1.035
R_1, wR_2 [$I > 2\sigma(I)$][a]	0.0185/0.0411	0.0221/0.0563
R_1, wR_2 (all data)	0.0199/0.0415	0.0222/0.0564
Largest difference peak and hole (e Å^{-3})	0.562 and −1.188	2.362 and −2.569

[a] $R_1 = \sum||F_o| - |F_c||/\sum|F_o|$; w$R_2 = [\sum w(F_o^2 - F_c^2)^2/\sum w(F_o^2)^2]^{1/2}$.

strated the corresponding elements in $Ce_2F_2(SO_4)_3{\cdot}2H_2O$ and $Ce_3F_4(SO_4)_4$.

Infrared spectroscopy

Infrared spectra of $Ce_2F_2(SO_4)_3{\cdot}2H_2O$ and $Ce_3F_4(SO_4)_4$ were obtained using a Nicolet iS10 Fourier transform IR spectrometer in the range of 400–4000 cm^{-1} and with a resolution of 4 cm^{-1}.

UV-Vis-NIR diffuse reflectance spectra

A Cary 5000 UV-Vis-NIR spectrophotometer was used for recording optical diffuse-reflectance spectra in the range 200–2500 nm and $BaSO_4$ samples were employed as the standard material.

Thermal analysis

Thermogravimetric analyses of $Ce_2F_2(SO_4)_3{\cdot}2H_2O$ and $Ce_3F_4(SO_4)_4$ were determined with a Netzsch STA 409PC thermal analyzer in the range 30–900 °C under flowing N_2.

Second-order NLO measurements

Measurements of SHG intensities for $Ce_3F_4(SO_4)_4$ were performed on a Q-switched Nd:YAG laser with a 1064 nm incident laser based on the method of Kurtz–Perry.[43] Because SHG signals depend significantly on particle sizes, the crystals of $Ce_3F_4(SO_4)_4$ were sieved into several particle size ranges (<26, 26–50, 50–74, 74–105, 105–150, 150–200 and 200–280 μm). Crystalline KDP with the corresponding size was used as the standard for comparison.

Computational descriptions

First-principles simulations for $Ce_3F_4(SO_4)_4$ were calculated with the CASTEP package,[44] using the pseudopotential density functional theory (DFT).[45] The generalized gradient approximation function proposed *via* Perdew, Burke, and Ernzerhof was utilized for depicting the correlation-exchange energy.[46,47] Optimal norm-conserving pseudopotential[48] with Kleinman–Bylander form was applied to model the relationship between the valence electron and the atom core, so that a smaller plane-wave basis set could be utilized without influencing the computational accuracy. More computational descriptions are shown in the ESI.†

Results and discussion

Structure description

The compound $Ce_2F_2(SO_4)_3{\cdot}2H_2O$ crystallizes in CS space group *Pbcn* of the orthorhombic crystal system and its asymmetric unit contains one Ce atom, two S atoms, one F atom, seven O atoms and two H atoms (Fig. S3a†). An eight-fold coordinated Ce^{4+} cation is bound to six O atoms (five O atoms from five $[SO_4]$ groups and one O atom from one H_2O), and two F atoms, forming a distorted $[CeO_6F_2]$ polyhedron with Ce–O bond lengths ranging from 2.219(3) to 2.394(3) Å and Ce–F distances in the range 2.193(2)–2.243(2) Å (Fig. 1a and Table S1†). Contiguous $[CeO_6F_2]$ units are connected with corner-sharing fluorine [F(1)] to form a 1D $[CeF]_\infty$ linear chain. Four-fold coordinated $[S(1)O_4]$ groups not only cap two adjacent $[CeO_6F_2]$ polyhedra to form three-membered rings $[Ce_2S]$ but also serve as linkers to construct double-layer $[Ce_2F_2(SO_4)_2]_\infty$ with a distance of 5.66 Å (Fig. 1b and c). The $[S(2)O_4]$ groups connected the adjacent double layers with an interlayer distance of 6.32 Å to build the final 3D structure (Fig. 1d and S4†). The purity of $Ce_2F_2(SO_4)_3{\cdot}2H_2O$ was determined using PXRD analysis, matching the simulations of single-crystal X-ray diffraction (Fig. S1a†). EDS studies further confirmed the presence of Ce, F, S, and O in $Ce_2F_2(SO_4)_3{\cdot}2H_2O$ (Fig. S2a†). Bond valence sum (BVS) calculations on Ce^{4+}, S^{6+}, O^{2-}, and F^- afford values of 3.80, 6.09–6.12, 1.61–2.04, and 1.10, respectively (Table S4†).

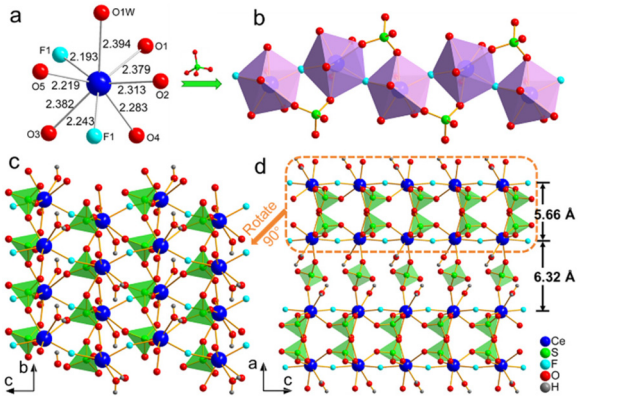

Fig. 1 (a) Coordination environment of the Ce atom and (b) 1D $[CeF(SO_4)]_\infty$ chain in $Ce_2F_2(SO_4)_3{\cdot}2H_2O$. (c) View of the $[Ce_2F_2(SO_4)_2]_\infty$ double layer in *bc*-plane. (d) The final 3D structure of $Ce_2F_2(SO_4)_3{\cdot}2H_2O$.

$Ce_3F_4(SO_4)_4$ crystallizes in a monoclinic crystal system of NCS and polar space group *C*2. Its asymmetric unit contains two independent Ce atoms, two S atoms, two F atoms, and eight O atoms (Fig. S3b†). A Ce(1) atom is octahedrally coordinated with five O atoms from five $[SO_4]$ units and three F atoms, forming a $[CeO_5F_3]$ polyhedron with Ce–O bonds ranging from 2.260(5) to 2.395(4) Å and Ce–F bonds in the range 2.245(6)–2.294(4) Å (Fig. 2a and Table S2†). An eight-fold coordinated Ce(2) atom is attached to six O atoms from six $[SO_4]$ units and two F atoms, constructing a $[CeO_6F_2]$ polyhedron, in which the ranges of Ce–O and Ce–F distances are 2.309(5) to 2.359(5) Å and 2.192(4)–2.192(4) Å, respectively (Fig. 2a and Table S2†). Notably, the adjacent atoms of Ce(1) and Ce(2) are connected *via* corner-sharing fluorine [F(2)], and Ce(1) and Ce(1) are bridged by fluorine [F(1)], constructing a 2D $[Ce_3F_4]_\infty$ layer with an interlayer distance of 6.06 Å (Fig. S5† and Fig. 3b). Two crystallographically independent $[SO_4]$ units cap the three-membered rings $[Ce_2S]$ between contiguous corner-sharing connected $[CeO_5F_3]$ and $[CeO_6F_2]$ polyhedra (Fig. 2b), and further serve as interlayer linkers to construct the final 3D framework (Fig. 2c). The purity was determined by PXRD studies (Fig. S1b†), and EDS analysis verified the coexistence of Ce, F, S, and O in $Ce_3F_4(SO_4)_4$ (Fig. S2b†). The BVS

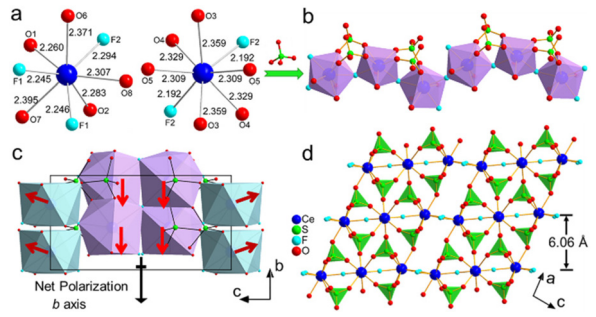

Fig. 2 (a) Coordination environments of Ce atoms. (b) 1D chain in $Ce_3F_4(SO_4)_4$. (c) View of the dipole orientation (red arrow) of the $[CeO_5F_3]$ and $[CeO_6F_2]$ polyhedra within one unit cell. The black arrows represent the direction of sum polarizations. (d) The final 3D structure of $Ce_3F_4(SO_4)_4$.

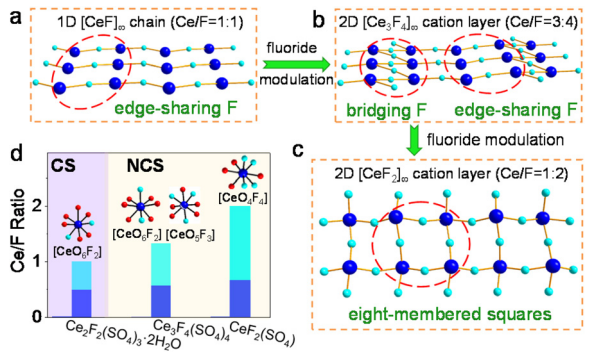

Fig. 3 Schematic diagrams of modulation fluorinated degree for 1D $[CeF]_\infty$ linear chains in $Ce_2F_2(SO_4)_3{\cdot}2H_2O$ (a), 2D $[Ce_3F_4]_\infty$ layer in $Ce_3F_4(SO_4)_4$ (b), and $[CeF_2]_\infty$ network-layered structure in $CeF_2(SO_4)$ (c). Oxygen atoms have been omitted for clarity. (d) Ce/F ratios and Ce-centered polyhedra of the three cerium fluoride sulfates.

results show values of 3.74–3.82, 6.11, 1.90–2.07, and 1.02–1.03 for Ce, S, O, and F, respectively (Table S4†).

Fluorination degree influencing macroscopic centricities and crystal structures

The combinations of tetravalent rare-earth cerium cations, fluorine anions, and sulfate groups have resulted in a wide variety of tetravalent rare-earth-metal fluorinated sulfates, including $Ce_2F_2(SO_4)_3{\cdot}2H_2O$, $Ce_3F_4(SO_4)_4$ and the reported $CeF_2(SO_4)$.[38] These three compounds possess a similar composition, but they exhibit distinct centricities and crystal structures under the modulation of the cerium–fluorine cationic framework. Structural transformations occur in the tetravalent rare-earth-metal fluorinated sulfates with different fluorination degrees, that is, the ratios of Ce/F, proceeding from 1.0 to 2.0, which may lead to the following three changes in the molecular structural arrangement (Fig. 3): (1) eight-fold coordinated Ce^{4+} cations possess various coordination modes, such as $[CeO_6F_2]$ polyhedra for $Ce_2F_2(SO_4)_3{\cdot}2H_2O$, $[CeO_5F_3]$ and $[CeO_6F_2]$ polyhedra for $Ce_3F_4(SO_4)_4$, and $[CeO_4F_4]$ polyhedra for $CeF_2(SO_4)$, which facilitate the generation of rich structural chemistry in cerium fluoride sulfates (Fig. 3d); (2) the different stoichiometric ratios (the ratios of Ce/F) can influence the dimension of framework structures by fluorination degree modulation, such as 1D $[CeF]_\infty$ linear chains in the $Ce_2F_2(SO_4)_3{\cdot}2H_2O$, 2D $[Ce_3F_4]_\infty$ layer in $Ce_3F_4(SO_4)_4$, and the 2D $[CeF_2]_\infty$ network-layered structure in $CeF_2(SO_4)$ (Fig. 3a–c); and (3) the cerium–fluorine cationic frameworks play a significant role in structural modification, including the symmetry and the geometric configuration. Dipole moment calculations for $Ce_3F_4(SO_4)_4$ demonstrate that the 2D $[Ce_3F_4]_\infty$ layer has a positive effect on reducing the molecular symmetry of Ce-centered polyhedra and displays a relatively large net dipole moment (−3.5 D) along the *b* axis (Fig. 2c).

Thermal analyses

Although $Ce_2F_2(SO_4)_3{\cdot}2H_2O$ and $Ce_3F_4(SO_4)_4$ have similar compositions, thermogravimetric analyses show completely different thermal behaviors. $Ce_2F_2(SO_4)_3{\cdot}2H_2O$ is thermally stable up to 170 °C only, which is attributed to the presence of two bound-water molecules (Fig. S6a†). Also, the thermal decomposition of $Ce_2F_2(SO_4)_3{\cdot}2H_2O$ shows three weight-loss steps. The weight loss of 5.61% in the temperature range of 170–340 °C is consistent with the removal of H_2O (calculated value: 4.83%). The weight loss (9.61%) ranging from 390 to 520 °C is attributed to the elimination of F_2 and O_2 (calculated value: 9.17%). The third stage (620–850 °C) shows a major weight loss of 29.91%, corresponding to the loss of SO_2 (calculated value: 30.67%). The final residuals of $Ce_2F_2(SO_4)_3{\cdot}2H_2O$ at 900 °C are measured using PXRD analysis, which are confirmed to be mainly CeO_2 and CeF_3 (Fig. S7a†). The TGA curve of $Ce_3F_4(SO_4)_4$ shows thermal stability up to 260 °C and a two-step weight loss stage (Fig. S6b†): the first stage (260–560 °C) exhibits a weight loss of 11.58%, consistent with the elimination of F_2 and O_2 (calculated value: 12.57%); and the second stage (600–850 °C) shows a major weight loss of 29.09%, corresponding to the loss of SO_2 (calculated value: 30.88%). The final residuals of $Ce_3F_4(SO_4)_4$ at 900 °C are confirmed to be mainly CeO_2 (Fig. S7b†).

Optical properties

Infrared spectra of $Ce_2F_2(SO_4)_3{\cdot}2H_2O$ and $Ce_3F_4(SO_4)_4$ have shown that the strong absorption bands for the two compounds ranging from 1200 to 800 cm^{-1} are consistent with ν_3 $[SO_4]^{2-}$ asymmetric stretching and ν_1 $[SO_4]^{2-}$ symmetric stretching (Fig. S8†).[49] The broad absorption bands for $Ce_2F_2(SO_4)_3{\cdot}2H_2O$ at 3555, 3474, and 1585 cm^{-1} demonstrate the existence of H_2O molecules.[50,51] Other bands (700–410 cm^{-1}) for the two compounds are attributed to the Ce–O/F asymmetric vibrations. The UV-Vis-NIR diffuse reflectance spectra for $Ce_2F_2(SO_4)_3{\cdot}2H_2O$ and $Ce_3F_4(SO_4)_4$ are shown in Fig. S9†, and the spectrum data were converted to band gaps with the Kubelka–Munk function: $F(R) = (1 - R)^2/2R = K/S$.[52] The optical band gaps for $Ce_2F_2(SO_4)_3{\cdot}2H_2O$ and $Ce_3F_4(SO_4)_4$ are 2.70 and 2.50 eV, respectively, corresponding to the yellow color of $Ce_2F_2(SO_4)_3{\cdot}2H_2O$ and $Ce_3F_4(SO_4)_4$ crystals. The experimental birefringence, as a significant linear-

optical property, is essential for assessing the phase-matching ability, and we have performed the birefringence measurement for $Ce_3F_4(SO_4)_4$ (Fig. S10†). A single crystal of $Ce_3F_4(SO_4)_4$ with high quality was produced to measure the birefringence using a ZEISS Axio A1 polarizing microscope. The crystal thickness (T) was 43.049 μm (Fig. S10d†), and the experimental retardation (ΔR) at 546 nm was measured to be about 6.06 μm by the positive and negative rotation of compensatory (Fig. S10a–S10c†). The birefringence of $Ce_3F_4(SO_4)_4$ was 0.141@546 nm, derived from the function $\Delta R = |Ne - No| \times T = \Delta n \times T$, which further proves its excellent linear-optical properties.

SHG properties

Power SHG intensities were measured on the crystalline sample of $Ce_3F_4(SO_4)_4$ owing to its NCS structure. The power SHG measurements show that $Ce_3F_4(SO_4)_4$ has a SHG effect of 1.0 × KDP in 1064 nm laser radiation (particle size, 105–150 μm) (Fig. 4). Notably, the SHG response gradually enhanced and finally reached a maximum value with the increase in particle sizes, demonstrating the phase-matchable behavior of $Ce_3F_4(SO_4)_4$. The SHG response of $Ce_3F_4(SO_4)_4$ is superior to the majority of reported fluorine-containing sulfate-based NLO materials, such as $Rb_6Sb_4F_{12}(SO_4)_3$ (0.1 × KDP),[37] $K_2SO_4{\cdot}SbF_3$ (0.1 × KDP),[53] $Rb_2SO_4{\cdot}SbF_3$ (0.3 × KDP),[53] $Rb_2SO_4{\cdot}(SbF_3)_2$ (0.5 × KDP),[54] and $RbSbF_2(SO_4)$ (0.96 × KDP),[55] being surpassed only by $CsSbF_2(SO_4)$ (3.0 × KDP)[28] and $CeF_2(SO_4)$ (8.0 × KDP).[38]

Theoretical calculations

First-principles simulations of $Ce_3F_4(SO_4)_4$ have been performed to elucidate electronic structure and property relationship.[41] The calculated energy band gap is 1.18 eV according to the DFT method in $Ce_3F_4(SO_4)_4$, which is smaller than the measured result owing to the derivative discontinuity of exchange–correlation energy (Fig. S11†). To gain deep insights into the origin of NLO properties, partial density of state (PDOS) and total DOS of $Ce_3F_4(SO_4)_4$ were performed (Fig. 5). The PDOS diagrams of $Ce_3F_4(SO_4)_4$ show that the states of Ce atoms overlap well with the O and F atoms in the whole energy region, exhibiting the highly covalent characters of the Ce–F and Ce–O bonds. The VB maximum is mostly defined through O-2p nonbonding orbitals, while Ce-4f states and some S-3p orbitals dominate the CB minimum. Therefore, these results

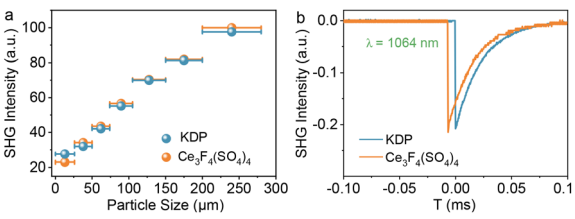

Fig. 4 (a) Phase-matching curves for $Ce_3F_4(SO_4)_4$ at 1064 nm laser radiation. Crystalline KDP with corresponding sizes were used as the standard for comparison. (b) Oscilloscope traces of SHG response for $Ce_3F_4(SO_4)_4$ with particle size ranging from 105 to 150 μm.

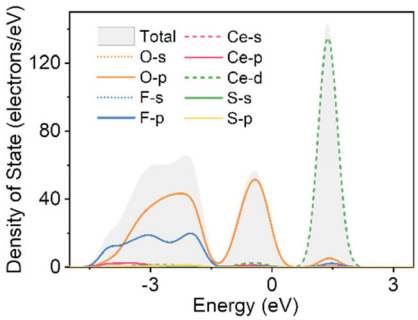

Fig. 5 DOS and PDOS diagrams for $Ce_3F_4(SO_4)_4$. Fermi levels are located at zero.

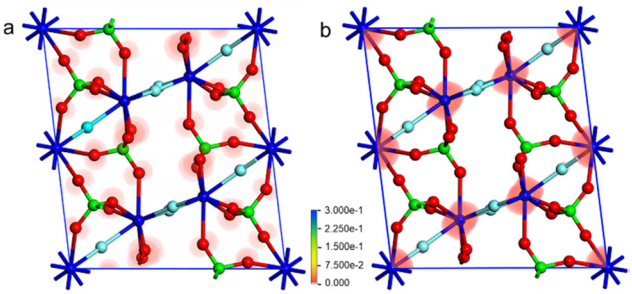

Fig. 6 SHG-weighted densities for (a) occupied and (b) unoccupied electronic states of $Ce_3F_4(SO_4)_4$.

demonstrate that the $[CeO_5F_3]$ polyhedra, $[CeO_6F_2]$ polyhedra and $[SO_4]$ groups determine the band gap of $Ce_3F_4(SO_4)_4$.

The calculated birefringence of $Ce_3F_4(SO_4)_4$ was about 0.096 at 1064 nm, consistent with the measured birefringence value, which further confirms the good phase-matching tendency observed in SHG experiments (Fig. S12†). Due to the restriction of space group $C2$, there are four non-zero independent SHG coefficients for $Ce_3F_4(SO_4)_4$, which are shown as follows: d_{12} = 5.95 pm V^{-1}, d_{14} = 4.67 pm V^{-1}, d_{22} = 1.90 pm V^{-1}, and d_{23} = 7.26 pm V^{-1}. The largest SHG tensor was larger than the measured value because the frequency of double light at 532 nm was partly absorbed. To better understand the contribution of electronic orbitals for the SHG response, the SHG-weighted electronic density simulations were carried out, which show that SHG-weighted electronic clouds are mostly localized on the $[CeF_3O_5]$, $[CeF_2O_6]$ and $[SO_4]$ units. For the occupied states, the nonbonding O-2p orbitals play a dominant role in SHG efficiency (Fig. 6a), while the SHG response is determined by Ce-4f states in unoccupied states (Fig. 6b), indicating that the units of $[CeF_3O_5]$ and $[CeF_2O_6]$ afford the main contribution to the SHG effect compared with $[SO_4]$ groups.

Conclusions

In summary, based on the CS model compound $Ce_2F_2(SO_4)_3{\cdot}2H_2O$, a cationic framework assembly strategy was

employed in the successful construction of the NCS polar $Ce_3F_4(SO_4)_4$ *via* fluorination degree modulation, which shows good linear and nonlinear optical performance including a large SHG effect of 1.0 × KDP and sufficient birefringence (0.141@546 nm) in fluorine-containing sulfate-based NLO materials. These results provide a new idea for introducing highly distorted fluorinated polyhedra to enhance the SHG effect of sulfate-based NLO crystals. More importantly, the work may open a door to efficiently develop new polar NCS materials by a cationic framework assembly strategy according to CS structures and accelerate the development of new structure-driven functional NLO materials.

Conflicts of interest

There are no conflicts to declare.

Acknowledgements

This research was financially supported by the National Natural Science Foundation of China (Nos. 51432006, 52002276), the Ministry of Education of China for the Changjiang Innovation Research Team (No. IRT14R23), the Ministry of Education and the State Administration of Foreign Experts Affairs for the 111 Project (No. B13025), and the Innovation Program of Shanghai Municipal Education Commission. M. G. H. thanks the Australian Research Council for support (DP170100411).

References

1 D. F. Eaton, Nonlinear optical materials, *Science*, 1991, **253**, 281–287.
2 K. M. Ok, Toward the rational design of novel noncentrosymmetric materials: Factors influencing the framework structures, *Acc. Chem. Res.*, 2016, **49**, 2774–2785.
3 H. W. Yu, N. Z. Koocher, J. M. Rondinelli and P. S. Halasyamani, Pb_2BO_3I: A borate iodide with the largest second-harmonic generation (SHG) response in the $KBe_2BO_3F_2$ (KBBF) family of nonlinear optical (NLO) materials, *Angew. Chem., Int. Ed.*, 2018, **57**, 6100–6103.
4 C. Wu, X. X. Jiang, Z. J. Wang, L. Lin, Z. S. Lin, Z. P. Huang, X. F. Long, M. G. Humphrey and C. Zhang, Giant optical anisotropy in the UV-transparent 2D nonlinear optical material $Sc(IO_3)_2(NO_3)$, *Angew. Chem., Int. Ed.*, 2021, **60**, 3464–3468.
5 C. B. Jiang, X. X. Jiang, C. Wu, Z. P. Huang, Z. S. Lin, M. G. Humphrey and C. Zhang, Isoreticular design of $KTiOPO_4$-like deep-ultraviolet transparent materials exhibiting strong second-harmonic generation, *J. Am. Chem. Soc.*, 2022, **144**, 20394–20399.
6 M. Wen, H. P. Wu, S. C. Cheng, J. Sun, Z. H. Yang, X. H. Wu and S. L. Pan, Experimental characterization and first principles calculations of linear and nonlinear optical properties of two orthophosphates $A_3Al_2(PO_4)_3$ (A = Rb, K), *Inorg. Chem. Front.*, 2019, **6**, 504–510.
7 P. Becker, Borate materials in nonlinear optics, *Adv. Mater.*, 1998, **10**, 979–992.
8 P. S. Halasyamani and K. R. Poeppelmeier, Noncentrosymmetric oxides, *Chem. Mater.*, 1998, **10**, 2753–2769.
9 C. T. Chen, G. L. Wang, X. Y. Wang and Z. Y. Xu, Deep-UV nonlinear optical crystal $KBe_2BO_3F_2$—discovery, growth, optical properties and applications, *Appl. Phys. B*, 2009, **97**, 9–25.
10 C. T. Chen, Y. C. Wu, A. D. Jiang, B. C. Wu, G. M. You, R. K. Li and S. J. Lin, New nonlinear-optical crystal: LiB_3O_5, *J. Opt. Soc. Am. B*, 1989, **6**, 616–621.
11 G. D. Boyd, R. C. Miller, K. Nassau, W. L. Bond and A. Savage, $LiNbO_3$: An efficient phase matchable nonenar optical material, *Appl. Phys. Lett.*, 1964, **5**, 234–236.
12 J. D. Bierlein and H. Vanherzeele, Potassium titanyl phosphate: properties and new applications, *J. Opt. Soc. Am. B*, 1989, **6**, 622–633.
13 A. O. Okorogu, S. B. Mirov, W. Lee, D. I. Crouthamel, N. Jenkins, A. Y. Dergachev, K. L. Vodopyanov and V. V. Badikov, Tunable middle infrared downconversion in GaSe and $AgGaS_2$, *Opt. Commun.*, 1998, **155**, 307–312.
14 L. Li, Y. Wang, B. H. Lei, S. J. Han, Z. H. Yang, K. R. Poeppelmeier and S. L. Pan, A new deep-ultraviolet transparent orthophosphate $LiCs_2PO_4$ with large second harmonic generation response, *J. Am. Chem. Soc.*, 2016, **138**, 9101–9104.
15 C. Wu, X. X. Jiang, L. Lin, Y. L. Hu, T. H. Wu, Z. S. Lin, Z. P. Huang, M. G. Humphrey and C. Zhang, A congruent-melting mid-infrared nonlinear optical vanadate exhibiting strong second-harmonic generation, *Angew. Chem., Int. Ed.*, 2021, **60**, 22447–22453.
16 W. X. Bao, Z. Q. Zhou, H. X. Tang, R. B. Fu, Z. J. Ma and X. T. Wu, $KPb_3(o\text{-}C_5H_4NCOO)_2Cl_5$: A brand-new stable lead chloride with good comprehensive nonlinear optical performance, *Inorg. Chem. Front.*, 2022, **9**, 1830–1835.
17 M. Luo, F. Liang, Y. X. Song, D. Zhao, F. Xu, N. Ye and Z. S. Lin, $M_2B_{10}O_{14}F_6$ (M = Ca, Sr): Two noncentrosymmetric alkaline earth fluorooxoborates as promising next-generation deep-ultraviolet nonlinear optical materials, *J. Am. Chem. Soc.*, 2018, **140**, 3884–3887.
18 F. G. You, F. Liang, Q. Huang, Z. G. Hu, Y. C. Wu and Z. S. Lin, $Pb_2GaF_2(SeO_3)_2Cl$: Band engineering strategy by aliovalent substitution for enlarging bandgap while keeping strong second harmonic generation response, *J. Am. Chem. Soc.*, 2019, **141**, 748–752.
19 H. M. Liu, Q. Wu, X. X. Jiang, Z. S. Lin, X. G. Meng, X. G. Chen and J. G. Qin, $ABi_2(IO_3)_2F_5$ (A = K, Rb, and Cs): A combination of halide and oxide anionic units to create a large second-harmonic generation response with a wide bandgap, *Angew. Chem., Int. Ed.*, 2017, **56**, 9492–9496.
20 C. Wu, X. X. Jiang, Z. J. Wang, H. Y. Sha, Z. S. Lin, Z. P. Huang, X. F. Long, M. G. Humphrey and C. Zhang, UV solar-blind-region phase-matchable optical nonlinearity

and anisotropy in a Π-conjugated cation-containing phosphate, *Angew. Chem., Int. Ed.*, 2021, **61**, 14806–14810.

21 T. H. Wu, X. X. Jiang, C. Wu, Y. L. Hu, Z. S. Lin, Z. P. Huang, M. G. Humphrey and C. Zhang, Ultrawide bandgap and outstanding second-harmonic generation response by a fluorine-enrichment strategy at a transition-metal oxyfluoride nonlinear optical material, *Angew. Chem., Int. Ed.*, 2022, **61**, e202203104.

22 X. R. Yang, X. Liu, Z. J. Wang, X. B. Deng, H. J. Lu, Y. J. Li, X. F. Long, L. Chen and L. M. Wu, $Na_{1.5}Rb_{0.5}PO_3F{\cdot}H_2O$: Synthesis, properties, and stepwise reconstruction of the hydrogen bond network, *Inorg. Chem. Front.*, 2021, **8**, 4544–4552.

23 Y. L. Hu, C. Wu, X. X. Jiang, Z. J. Wang, Z. P. Huang, Z. S. Lin, X. F. Long, M. G. Humphrey and C. Zhang, Giant second-harmonic generation response and large band gap in the partially fluorinated mid-infrared oxide $RbTeMo_2O_8F$, *J. Am. Chem. Soc.*, 2021, **143**, 12455–12459.

24 J. Chen, C. L. Hu, F. F. Mao, J. H. Feng and J. G. Mao, A facile route to nonlinear optical materials: Three-site aliovalent substitution involving one cation and two anions, *Angew. Chem., Int. Ed.*, 2019, **58**, 2098–2102.

25 T. H. Wu, X. X. Jiang, C. Wu, H. Y. Sha, Z. J. Wang, Z. S. Lin, Z. P. Huang, X. F. Long, M. G. Humphrey and C. Zhang, From $Ce(IO_3)_4$ to $CeF_2(IO_3)_2$: Fluorinated homovalent substitution simultaneously enhances SHG response and bandgap for mid-infrared nonlinear optics, *J. Mater. Chem. C*, 2021, **9**, 8987–8993.

26 M. L. Liang, C. L. Hu, F. Kong and J. G. Mao, $BiFSeO_3$: An excellent SHG material designed by aliovalent substitution, *J. Am. Chem. Soc.*, 2016, **138**, 9433–9436.

27 F. F. Mao, C. L. Hu, X. Xu, D. Yan, B. P. Yang and J. G. Mao, $Bi(IO_3)F_2$: The first metal iodate fluoride with a very strong second harmonic generation effect, *Angew. Chem., Int. Ed.*, 2017, **56**, 2151–2155.

28 X. H. Dong, L. Huang, C. F. Hu, H. M. Zeng, Z. E. Lin, X. Wang, K. M. Ok and G. H. Zou, $CsSbF_2SO_4$: An excellent ultraviolet nonlinear optical sulfate with a $KTiOPO_4$ (KTP)-type structure, *Angew. Chem., Int. Ed.*, 2019, **58**, 6528–6534.

29 C. Wu, L. Lin, X. X. Jiang, Z. S. Lin, Z. P. Huang, M. G. Humphrey, P. S. Halasyamani and C. Zhang, $K_5(W_3O_9F_4)(IO_3)$: An efficient mid-infrared nonlinear optical compound with high laser damage threshold, *Chem. Mater.*, 2019, **31**, 10100–10108.

30 S. J. Han, M. Miriding, T. Abudukadi, Z. H. Yang and S. L. Pan, $PbB_5O_7F_3$: A high-performing short-wavelength nonlinear optical material, *Chem. Mater.*, 2020, **32**, 2172–2179.

31 R. H. Cong, Y. Wang, L. Kang, Z. Y. Zhou, Z. S. Lin and T. Yang, An outstanding second-harmonic generation material BiB_2O_4F: Exploiting the electronwithdrawing ability of fluorine, *Inorg. Chem. Front.*, 2015, **2**, 170–176.

32 M. Zhang, C. Hu, T. Abudouwufu, Z. H. Yang and S. L. Pan, Functional materials design via structural regulation originated from ions introduction: A study case in cesium iodate system, *Chem. Mater.*, 2018, **30**, 1136–1145.

33 L. Xiong, J. Chen, J. Lu, C. Y. Pan and L. M. Wu, Monofluorophosphates: A new source of deep-ultraviolet nonlinear optical materials, *Chem. Mater.*, 2018, **30**, 7823–7830.

34 J. Chen, C. L. Hu and J. G. Mao, $LiGaF_2(IO_3)_2$: A mixed-metal gallium iodate-fluoride with large birefringence and wide band gap, *Sci. China Mater.*, 2021, **64**, 400–407.

35 M. Q. Gai, T. H. Tong, Y. Wang, Z. H. Yang and S. L. Pan, New alkaline-earth metal fluoroiodates exhibiting large birefringence and short ultraviolet cutoff edge with highly polarizable $(IO_3F)^{2-}$ units, *Chem. Mater.*, 2020, **32**, 5723–5728.

36 W. Y. Zhang, W. Q. Jin, Z. H. Yang and S. L. Pan, $K_4(PO_2F_2)_2(S_2O_7)$: First fluorooxophosphorsulfate with mixed-anion $[S_2O_7]^{2-}$ and $[PO_2F_2]^{-}$ groups, *Dalton Trans.*, 2020, **49**, 17658–17664.

37 X. H. Dong, Y. Long, X. Y. Zhao, L. Huang, H. M. Zeng, Z. E. Lin, X. Wang and G. H. Zou, $A_6Sb_4F_{12}(SO_4)_3$ (A = Rb, Cs): Two novel antimony fluoride sulfates with unique crown-like clusters, *Inorg. Chem.*, 2020, **59**, 8345–8352.

38 C. Wu, T. H. Wu, X. X. Jiang, Z. J. Wang, H. Y. Sha, L. Lin, Z. S. Lin, Z. P. Huang, X. F. Long, M. G. Humphrey and C. Zhang, Large second-harmonic response and giant birefringence of $CeF_2(SO_4)$ induced by highly polarizable polyhedra, *J. Am. Chem. Soc.*, 2021, **143**, 4138–4142.

39 T. H. Wu, X. X. Jiang, Y. R. Zhang, Z. J. Wang, H. Y. Sha, C. Wu, Z. S. Lin, Z. P. Huang, X. F. Long, M. G. Humphrey and C. Zhang, From $CeF_2(SO_4){\cdot}H_2O$ to $Ce(IO_3)_2(SO_4)$: Defluorinated homovalent substitution for strong second-harmonic-generation effect and sufficient birefringence, *Chem. Mater.*, 2021, **33**, 9317–9325.

40 C. Wu, C. B. Jiang, G. F. Wei, X. X. Jiang, Z. J. Wang, Z. S. Lin, Z. P. Huang, M. G. Humphrey and C. Zhang, Toward large second-harmonic generation and deep-UV transparency in strongly electropositive transition metal sulfates, *J. Am. Chem. Soc.*, 2023, **145**, 3040–3046.

41 G. M. Sheldrick, *SHELXS-97: Program for the solution of crystal structures*, University of Göttingen, Germany, 1997.

42 A. L. Spek, Single-crystal structure validation with the program PLATON, *J. Appl. Crystallogr.*, 2003, **36**, 7–13.

43 S. K. Kurtz and T. T. Perry, A powder technique for the evaluation of nonlinear optical materials, *J. Appl. Phys.*, 1968, **39**, 3798–3813.

44 S. J. Clark, I. Segall, C. J. Pickard, P. J. Hasnip, M. I. J. Probert, K. Refson and M. C. Payne, First principles methods using CASTEP, *Z. Kristallogr.*, 2005, **220**, 567–570.

45 M. C. Payne, M. P. Teter, D. C. Allan, T. A. Arias and J. D. Joannopoulos, Iterative minimization techniques for ab initiototal-energy calculations: molecular dynamics and conjugate gradients, *Rev. Mod. Phys.*, 1992, **64**, 1045–1097.

46 J. P. Perdew, K. Burke and M. Ernzerhof, Generalized gradient approximation made simple, *Phys. Rev. Lett.*, 1996, **77**, 3865–3868.

47 J. P. Perdew and Y. Wang, Pair-distribution function and its coupling-constant average for the spin-polarized electron gas, *Phys. Rev. B: Condens. Matter Mater. Phys.*, 1992, **46**, 12947–12954.

48 D. R. Hamann, M. Schlüter and C. Chiang, Norm-conserving pseudopotentials, *Phys. Rev. Lett.*, 1979, **43**, 1494–1497.

49 F. F. He, Y. L. Deng, X. Y. Zhao, L. Huang, D. J. Gao, J. Bi, X. Wang and G. H. Zou, $RbSbSO_4Cl_2$: An excellent sulfate nonlinear optical material generated due to the synergistic effect of three asymmetric shromophores, *J. Mater. Chem. C*, 2019, **7**, 5748–5754.

50 T. Abudouwufu, M. Zhang, S. C. Cheng, Z. H. Yang and S. L. Pan, $Ce(IO_3)_2F_2{\cdot}H_2O$: The first rare-earth-metal iodate fluoride with large second harmonic generation response, *Chem. – Eur. J.*, 2019, **25**, 1221–1226.

51 C. Wu, X. X. Jiang, L. Lin, W. Y. Dan, Z. S. Lin, Z. P. Huang, M. G. Humphrey and C. Zhang, Strong SHG responsesina beryllium-free deep-UV-transparent hydroxyborate via covalent bond modification, *Angew. Chem., Int. Ed.*, 2021, **60**, 27151–27157.

52 W. M. Wendlandt and H. G. Hecht, *Reflectance Spectroscopy*, Interscience, New York, 1966.

53 F. F. He, L. Wang, C. F. Hu, J. Zhou, Q. Li, L. Huang, D. J. Gao, J. Bi, X. Wang and G. H. Zou, Cation-tuned synthesis of the $A_2SO_4{\cdot}SbF_3$ (A = Na^+, NH^{4+}, K^+, Rb^+) family with nonlinear optical properties, *Dalton Trans.*, 2018, **47**, 17486–17492.

54 Q. Wang, L. Wang, X. Y. Zhao, L. Huang, D. J. Gao, J. Bi, X. Wang and G. H. Zou, Centrosymmetric $K_2SO_4{\cdot}(SbF_3)_2$ and noncentrosymmetric $Rb_2SO_4{\cdot}(SbF_3)_2$ resulting from cooperative effects of lone pair and cation size, *Inorg. Chem. Front.*, 2019, **6**, 3125–3132.

55 F. Yang, L. J. Huang, X. Y. Zhao, L. Huang, D. J. Gao, J. Bi, X. Wang and G. H. Zou, An energy band engineering design to enlarge the band gap of $KTiOPO_4$ (KTP)-type sulfates via aliovalent substitution, *J. Mater. Chem. C*, 2019, **7**, 8131–8138.